

Tuning quaternary ammonium ionomer composition and processing to produce tough films

Wayz R. Khan, Nick Murdakes, Chris J. Cornelius*

Department of Chemical and Biomolecular Engineering, University of Nebraska - Lincoln, Lincoln, NE, 68588-0643, United States

ARTICLE INFO

Article history:

Received 4 December 2017

Received in revised form

8 March 2018

Accepted 14 March 2018

Available online 15 March 2018

Keywords:

Multiblock ionomer

Hydroxyl conductivity

Swelling and film strength

ABSTRACT

Multi-block and random quaternary ammonium poly (arylene ether sulfone) copolymer ionomers were synthesized using sequential reactions. Ionomer film processing involved two separate methods: heterogeneous-conversion and solution-casting a pseudo-solution. Film hydroxyl conductivity, water swelling, and tensile strength were dependent upon the hydrophilic and hydrophobic block-length. ^1H nuclear magnetic resonance was used to evaluate brominated multi-block poly (arylene ether sulfone) composition, degree of functionalization (DF), and ion-exchange capacity (IEC). In general, multi-block ionomer hydroxyl conductivity was greater than its randomly functionalized counterpart at a similar IEC. Multi-block ionomer films with largest hydrophilic block length exhibited a hydroxide conductivity of 49.8 mS/cm. However, the equivalent random copolymer's conductivity was 1.02 times lower with a water uptake of 223 wt%, which were 190% higher than its multi-block counterpart. This was attributed to ion-clustering improvements, which is not present in a random ionomer. Equivalent copolymer ionomers had a percolation threshold associated with excessive swelling when its IEC exceeded 2.02 meq/g. In contrast to the random ionomer, the maximum swelling observed for the multi-block copolymers was 33.6% at an IEC of 2.86 meq/g. This swelling suppression at high IEC was attributed to the sequential hydrophilic-hydrophobic block architecture. Moreover, the solution-cast multi-block ionomer was found to possess the highest toughness of $1185 \times 10^4 \text{ J/m}^3$, which was 237% greater than its heterogeneous counterpart. These results suggest that block length and ionomer processing play a critical role in controlling swelling, improving mechanical strength, and enhancing ion transport.

© 2018 Published by Elsevier Ltd.

1. Introduction

Over the last five decades, numerous researchers have been designing and synthesizing new ionomers in order to improve their physical, chemical, and transport properties [1–13]. An ionomer has three salient features: ion conduction, hydrophilicity, and fixed charge carriers within electrically neutral repeat units [14,15]. Ionomers are used as separation membranes in a wide variety of fields such as electrodialysis, electrolysis, diffusion-dialysis, batteries, sensing materials, biomedical, analytical chemistry, and proton exchange membrane (PEM) and anion exchange membrane (AEM) fuel cells [16–18].

Ionomer properties are linked to composition and a chain's spatial arrangement, which may lead to lamellar, cylindrical, or spherical morphologies [9,19–21]. For example, Lee [22] and Zhao

[23] showed that sulfonated poly (arylene ether ether ketone)-*b*-polyimide and poly (ether ether ketone) (SPEEK) copolymers with bigger block lengths facilitated a greater degree of phase separation leading to the formation of bigger hydrophobic domains and ion clusters. The resultant phase separated morphology with distinct hydrophilic and hydrophobic domains gave rise to a remarkable increase in proton transport properties as compared to random copolymers. In addition to ionomer backbone architecture, processing methodology has significant effects upon film properties. Casting solvent and film drying temperatures of Nafion [3] and SPEEK [24] resulted in large differences in proton transport and chemical stability. Bebin and Galiano [25,26] examined melt-cast and solvent-cast sulfonated polysulfone (SPSU) films. The results revealed that solvent-cast SPSU film's proton conductivity was two times greater than melt-cast one at the same ion-exchange capacity (IEC). Weiss [27] demonstrated that sulfonated block copolymers (S-SEBS) suffered from ion aggregate dissociation or microphase separation at lower temperatures as compared to similar

* Corresponding author.

E-mail address: ccornelius2@unl.edu (C.J. Cornelius).

homopolymers. This spherical microstructure became deformed during compression molding as compared to a Zn-S-SEBS solution-cast film. This film had a lamellar microstructure that was attributed to improved solvent-ionomer interactions. Lee et al. [28] studied the effect of block length and solution-casting on the morphology, physical properties, and proton conductivities of a disulfonated poly (arylene ether sulfone) multiblock copolymer. Fan and Cornelius et al. [29] explored ionomer block length effects upon the viscoelastic and gas transport properties of a series of sulfonated poly (arylene ether sulfone) multiblock copolymers (BPSH-BPS). The solution-casting effect upon poly (*t*-butylstyrene-*b*-ethylene-*alt*-propylene-*b*-sulfonated styrene-*b*-ethylene-*alt*-propylene-*b*-*t*-butyl styrene) in cyclohexane:heptane (C:H) and tetrahydrofuran (THF) were evaluated by Wen and Cornelius [9]. Solution-casting this pentablock copolymer (PBC) into a film using C:H versus THF altered its morphology that contained a random distribution of sulfonated domains to an ordered material with a mixture of cylinders and lamellae. Increased film morphological order improved its modulus and proton conductivity leading to better ionomeric polymer-metal composite (IPMC) actuation performance. All these studies reveal that solution-casting affects must be considered in order to create films with desirable properties based upon its composition.

Although these research efforts strongly suggest that ionomer processing has a critical role on its final properties, its importance has not been widely explored using an AEM. AEM films are typically prepared by two methods: heterogeneous and pseudo-homogeneous conversion. The first method involves converting a chloromethylated or brominated polymer solid into an AEM by immersion in a trimethylamine (TMA) solution at room temperature (25 °C). A solid-state Menshutkin reaction occurs within the film as the bromomethylbenzyl groups are converted to benzyl-trimethyl ammonium moieties. The film is converted into its hydroxide form by soaking in an alkaline solution. Ionomers formed by solid-state conversion are heterogeneous AEMs. A pseudo-homogeneous conversion method uses a TMA solution that is slowly added to a chloromethylated or brominated polymer solution. This produces a colloidal solution that is partly phase-separated, which is used to create a pseudo-solution-cast a film.

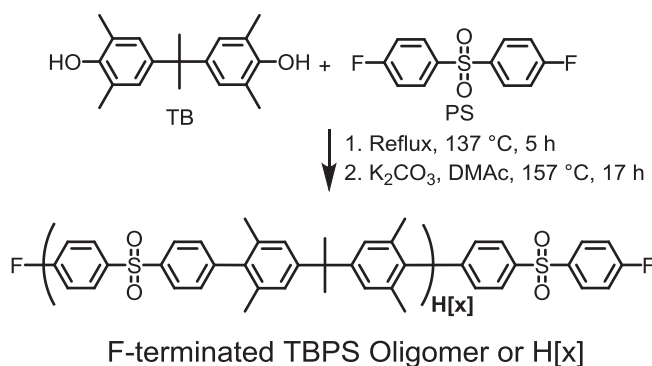
In this study, a series of multiblock quaternary ammonium (QA) ionomers was created using a poly (arylene ether sulfone) (PAES) to form AEM films based upon solid-state and pseudo-homogeneous conversion techniques. The heterogeneous and pseudo-solution-cast film physical properties were studied as a function of ion-exchange capacity (IEC) using nuclear magnetic resonance spectroscopy (NMR), electrochemical impedance spectroscopy (EIS), and dynamical mechanical analysis (DMA). It was found that pseudo-solution-casting a QA ionomer dramatically enhanced its tensile properties, swelling behavior, and stabilized ion transport properties as compared to its equivalent heterogeneous based AEM film. This effort highlights the importance of solvent to ionomer film processing and its effect upon improved AEM physical and transport properties.

2. Experimental

A series of multiblock PAES copolymers were synthesized from independently prepared F-terminated and OH-terminated oligomers using a nucleophilic substitution polycondensation reaction and controlled stoichiometric ratios during their synthesis.

2.1. Synthesis of hydrophilic precursor block (TBPS) with fluorine ends

The hydrophilic precursor block (TBPS) was synthesized terminated with fluorine ends was synthesized using tetramethyl



Scheme 1. TBPS or H [x] oligomer synthesis.

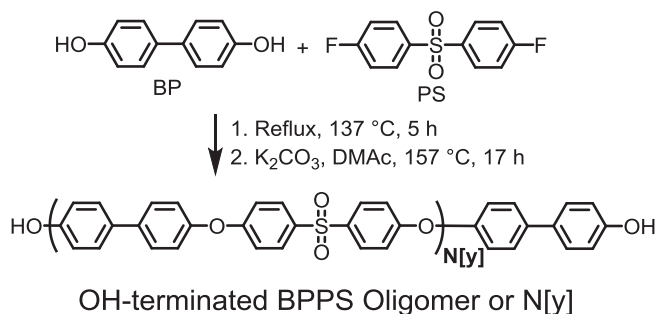
bisphenol-A (TB) and 4,4'-difluorodiphenyl sulfone (PS) shown in Scheme 1. A typical TBPS oligomer polymerization procedure used to create a 18 kg/mol number average molecular weight (M_n) block referred to as H [18k] is the following: A 300 mL three-necked, round-bottomed flask was washed and then flame dried prior to charging with TB (3.5549 g, 12.5 mmol), PS (3.4537 g, 13.6 mmol), and K_2CO_3 (2.5914 g, 18.8 mmol). The polymerization reaction was carried out in 60 mL of DMAc and 25 mL of toluene under an argon atmosphere in a round-bottomed flask equipped with Dean-Stark trap, condenser, mechanical stirrer, and gas inlet and outlet. The reaction temperature was maintained at 137 °C for 5 h before the toluene and residual water from the reaction solvent were removed from the system as an azeotrope by distillation. The reaction temperature was raised to 157 °C and preceded with vigorous stirring and argon flow (atmosphere) for 17 h. The oligomer block number average molecular weight (M_n) was determined using gel permeation chromatography (GPC).

2.2. Synthesis of hydrophobic block (BPPS) with hydroxyl ends

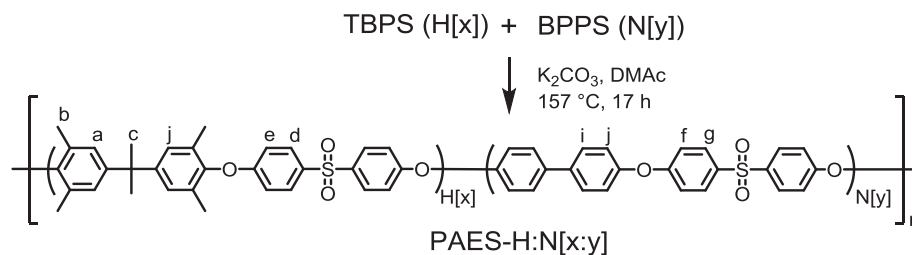
The hydroxyl-terminated BPPS block was synthesized using bisphenol-A (BP) and 4,4'-difluorodiphenyl sulfone (PS) shown in Scheme 2. The procedure for preparing a block with a M_n of 8 kg/mol that is referred to as N [8k] is the following: BP (1.7517 g, 94 mmol), PS (2.1164 g, 83 mmol), and K_2CO_3 (1.9503 g, 14.1 mmol), 35 mL DMAc and 15 mL toluene were placed into a washed, flame dried 250 mL three-necked round-bottomed flask. The mixture was refluxed at 137 °C under argon flow for 5 h. After removal of the residual water from the system, the mixture was maintained at 157 °C for another 17 h with continuous stirring and argon flow. The oligomer M_n was evaluated using GPC.

2.3. TBPS and BPPS copolymerization

TBPS and BPPS oligomer copolymerization was done to produce



Scheme 2. BPPS or N [y] oligomer synthesis.



Scheme 3. Synthesis of TBPS-BPPS multiblock PAES-H:N [x:y].

Table 1
PAES-H:N [x:y] block size, overall Mn, and PDI.

Sample	TBPS (g/mol)	BPPS (g/mol)	M _n [*] (g/mol)	PDI [*]
PAES-H:N [3k:2k]	3.0k	2.0k	21.0k	1.48
PAES-H:N [6k:9k]	6.0k	9.0k	21.2k	1.29
PAES-H:N [6k:5k]	6.0k	5.0k	28.6k	1.29
PAES-H:N [6k:3k]	6.0k	3.0k	45.9k	1.48
PAES-H:N [12k:31k]	12k	31k	34.4k	1.48
PAES-H:N [12k:19k]	12k	17k	22.6k	1.69
PAES-H:N [12k:11k]	12k	11k	72.1k	1.63
PAES-H:N [18k:8k]	18k	8.0k	31.9k	1.75
PAES-H:N [24k:39k]	24k	39k	37.1k	1.52
PAES-H:N [24k:23k]	24k	23k	47.8k	1.52
PAES-H:N [34k:14k]	34k	14k	48.8k	1.56

* Determined by GPC.

a multiblock PAES shown in Scheme 3. Hydroxy-terminated BPPS block (N [8k]) was reacted with a stoichiometric amount of fluoro-terminated TBPS block (H [18k]) at 157 °C for 17 h under argon. After cooling to 25 °C, the mixture was centrifuged and precipitated in 200 mL of methanol. A fibrous polymer solid was collected by filtration, washed with ethanol, and then it was dried in a vacuum oven at 50 °C for 12 h. This multiblock PAES-H:N [18k:8k] copolymer had a Mn of 31.9 kg/mol and polydispersity index (PDI) of 1.75 determined using GPC. The non-functionalized multiblock copolymer's initial oligomer mass, overall Mn, and PDI are summarized in Table 1. All copolymers produced optically clear films that were creasable and tough due to sufficiently high molecular weight. No oligomers or their blends in this series were film-forming.

2.4. Bromination of PAES-H:N[x:y]

Multiblock PAES copolymers were controllably brominated using *N*-bromosuccinimide (NBS) as the bromination agent and benzoyl peroxide (BPO) as the initiator for the radical reaction in 1,1,2,2-tetrachloroethane (TCE). The procedure for preparing brominated PAES-H:N [x:y] is described by the following: 1.0 g of PAES-H:N [18k:8k] polymer, 1.3349 g of NBS (7.5 mmol), and 0.0454 g of BPO (1.9 mmol) were dissolved in 15 mL of TCE in a three-necked round-bottomed flask equipped with a mechanical stirrer and a condenser. The solution was then slowly heated to 80 °C under argon flow. When the mixture reached 80 °C, TCE began to reflux and the mixture turned blood red. After 3 h, the reaction mixture was cooled to 25 °C and poured into excess ethanol. The yellow fibrous precipitate was collected by filtration, washed with water, and dried in vacuum at 35 °C to yield a tan brown solid (1.21 g). NBS concentration was controlled in order to obtain a targeted IEC for Br-PAES-H:N [x:y].

2.5. Quaternization and film formation

QPAES-H:N [x:y] ionomer films were prepared from Br-PAES-

H:N [x:y] using two separate methods: heterogeneous conversion and pseudo-solution casting. Br-PAES-H:N [x:y] films were created by solution casting from a 5–10 wt% polymer in CH₂Cl₂. The solvent was controllably evaporated from the solution in a chemical fume hood at 25 °C for 12 h until a dense film was formed on it. The Br-PAES-H:N [x:y] film was converted into an ionomer by solid-state conversion using a 50% (w/w) TMA solution within a sealed container for 48 h at 25 °C to yield a heterogeneous (*h_T*) film. The bromomethylbenzyl group conversion into a benzyl-trimethylammonium moiety occurred via a heterogeneous Menshutkin reaction. The quaternized films were soaked in 0.5 M NaOH for 48 h at 25 °C to replace all the bromide ions with hydroxide ones. The *h_T* films were completely rinsed and immersed in deionized water for 48 h to remove any residual NaOH.

The second film-forming technique utilized a QA ionomer colloidal-dispersion (*s_C*) that was solution-cast using DMAc. A 5–10 wt% QA ionomer solution was created from a QPAES-H:N [x:y] that was produced by solid state using TMA and the Menshutkin reaction. A colloidal-dispersion was generated after vigorously stirring a QA ionomer in DMAc. A *s_C*-QPAES-H:N [x:y] film was created by solution casting it on a glass substrate at 50 °C under vacuum for 48 h. The subsequent *s_C*-QPAES-H:N [x:y] film was peeled off the glass using water and converted into its hydroxide form by immersion in 0.5 M NaOH solution for 48 h. The *s_C* films were thoroughly washed and placed in deionized water for 48 h.

Due to high CO₂ sensitivity, the hydroxide ion rapidly converts to CO₃²⁻/HCO₃⁻ upon exposure to air. For this reason, material characterization in the hydroxide form is very difficult. Therefore, both *h_T* and *s_C* films were converted to bicarbonate form by exposure to CO₂ in air for 72 h. All films were in the bicarbonate form and stored in deionized water before analysis.

2.6. Characterization and measurements

2.6.1. ¹H NMR, FT-IR and GPC

¹H NMR spectra were obtained on a Bruker Avance NMR spectrometer operating at a proton frequency of 400 MHz. Deuterated chloroform (CDCl₃) was the NMR solvent for brominated copolymer samples and deuterated dimethyl sulfoxide (DMSO-d₆) were used for quaternized samples. Tetramethylsilane (TMS) was used as an internal reference.

FT-IR spectra were collected to confirm the pendant functional groups on the multiblock copolymer. FT-IR absorption spectra of the films were obtained using a Thermo-Nicolet 380 FT-IR spectrometer with a resolution of 0.4 cm⁻¹ that was equipped with an ATR accessory. Measurements were recorded on film samples of thickness 30–50 μm.

GPC data was collected using a PSS, SECurity system equipped with an isocratic pump, autosampler and a refractive index detector. The system uses tetrahydrofuran as the mobile phase and was operated at 25 °C with a flow rate of 1.0 mL/min. Molecular weight's were determined from a calibration plot constructed using

polystyrene standards.

2.6.2. DF and IEC

Material IEC and DF were evaluated by taking the ratio of the integrals in the ^1H NMR spectra for the protons in the bromobenzylmethyl group (l' in Scheme 4) to the sum of the integrals from the bromobenzylmethyl protons and remaining benzylmethyl protons ($l' + b'$ in Scheme 1). IEC was determined from DF and the ratio of the ^1H NMR peaks from bromobenzyl and benzylmethyl protons (l' and b') assuming complete quaternization (see Scheme 5)

2.6.3. Ionomer film water uptake and conductivity

The ionomer's dry mass (M_{dry}) was determined after drying at 50°C under vacuum for 24 h. The film's wet mass (M_{wet}) was measured after equilibrating a film in deionized water. The mass was measured after quickly removing surface water and weighing immediately afterwards. Water uptake (WU) values were determined using Equation (1) based upon three different samples. These results are summarized in Table 2 with a variability of less than 10%, which indicates statistically significant changes between samples based upon IEC and processing technique.

$$\text{WU} = \frac{M_{\text{wet}} - M_{\text{dry}}}{M_{\text{dry}}} \times 100\% \quad (1)$$

Nyquist impedance plots of fully hydrated ionomer films were collected using a Metrohm Autolab PGSTAT302 N from 10^{-3} – 10^6 Hz. A two-probe method was used to measure its resistance (R) in the plane of the film with a BekkTech LLC test cell (Teflon cell). The film's bulk R was obtained from a Nyquist impedance plot by interpolating the high-frequency arc to the x-axis. A rectangular sample with a nominal width between 4 and 5 mm was placed in a Teflon cell, where it was clamped between Pt wire electrodes. The distance between Pt electrodes was $L = 0.5$ cm, and the film's cross-sectional area was A . Test temperature was controlled using an isothermal water bath (Thermo Scientific Inc.). Film thickness was measured in its swollen state prior to an impedance test. Fully hydrated ionomer film conditions were created by submerging a film and allowing it to equilibrate in deionized water. Film conductivity (σ) values were calculated based on five measurements. The samples in-plane σ was calculated from Equation (2). These results are summarized in Table 2 based upon three to five different samples with a variability of less than 2%, which indicates statistically significant changes between samples based upon IEC and processing technique.

$$\sigma = \frac{L}{RA} \quad (2)$$

2.6.4. Swelling ratio

The film's swelling ratio (SR) was determined from rectangular

samples ($5\text{ mm} \times 10\text{ mm}$) based upon their initial dry dimensions and after equilibrating in deionized water. A dry film's thickness (t_{dry}) and length (L_{dry}) were evaluated after drying in vacuum oven at 50°C for 24 h. A dried film was equilibrated in H_2O at 25°C for a minimum of 24 h before measuring its fully hydrated wet length (L_{wet}) and thickness (t_{wet}). The dry and wet film's dimensional changes were evaluated using a Vernier scale. The film's SR was calculated using Equation (3) based upon three different samples with a variability of less than 10%. This indicates statistically significant changes between sample series based upon IEC and processing technique. These SR results are summarized in Table 3.

$$\text{SR}(\%) = \frac{L_{\text{wet}} - L_{\text{dry}}}{L_{\text{dry}}} \times 100\% \quad (3)$$

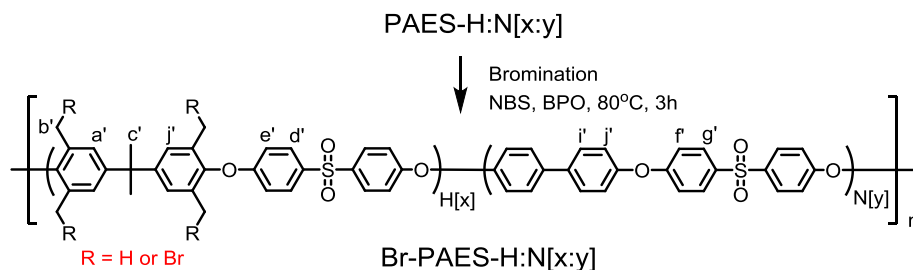
2.6.5. Stress-strain measurements

Hydrated QPAES-H:N [x:y] films in their bicarbonate form were evaluated for toughness, elongation at break, and Young's modulus at 25°C . Hydrated samples were taken out of deionized water and gently swabbed with lab wipes to remove any surface moisture before testing. A TA Instrument Q800 Dynamic Mechanical Analyzer (DMA) was used to measure stress-strain behavior based upon films with a nominal length, width, and thickness of 7.5 mm, 3.5 mm, and 0.05 mm. The tension experimental parameters were a preload force of 0.001 N, a 0.01% initial strain, and a displacement rate $500\ \mu\text{m}/\text{min}$. All test results are based upon a minimum of four individual test measurements that was used to calculate its standard deviation.

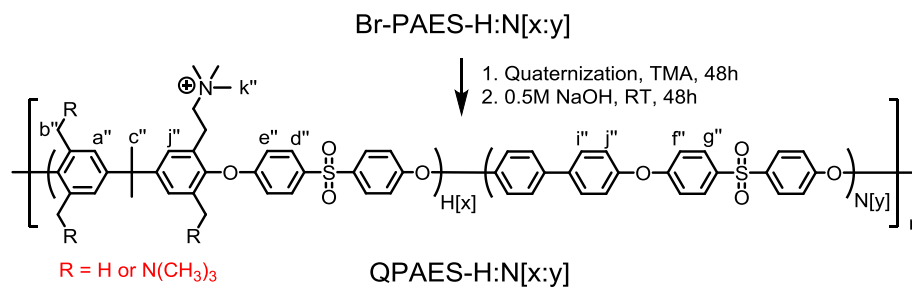
3. RESULTS AND DISCUSSION

3.1. ^1H NMR and FT-IR of ionomer films

PAES-H:N [x:y], Br-PAES-H:N [x:y], and QPAES-H:N [x:y] were studied using ^1H NMR to confirm its chemical structure and composition. An example ^1H NMR spectra using PAES-H:N [18k:8k], Br-PAES-H:N [18k:8k], and QPAES-H:N [18k:8k] are shown in Fig. 1. A new peak (l') appeared at $\delta = 4.35$ ppm that is the bromobenzyl protons ($\text{Ar}-\text{CH}_2\text{Br}$) after PAES-H:N [18k:8k] conversion into Br-PAES-H:N [18k:8k]. The aromatic ring's proton signals ranged from 6.7 to 8.0 ppm, and the gem dimethyl group's proton associated with the benzylmethyl (c') was observed at $\delta = 1.75$ ppm. The Br-PAES-H:N [x:y] copolymer's DF was calculated based upon the bromobenzyl group (l') integral ratio to the benzylmethyl and bromobenzyl group ($l' + b'$) sum. These values ranged from 0.71 to 3.40 summarized in Table 2. Bromobenzyl conversion to a benzyltrimethyl ammonium group was accomplished by submerging a Br-PAES-H:N [x:y] film into an aqueous TMA solution (50 wt%) for 48 h. The subsequent QPAES-H:N [x:y] ionomer ^1H NMR spectra was obtained by dissolving in DMSO- d_6



Scheme 4. PAES-H:N [x:y] bromination to create Br-PAES-H:N [x:y].



Scheme 5. Br-PAES-H:N [x:y] quaternization into QPAES-H:N [x:y] using TMA.

Table 2

Multiblock QA ionomer film water uptake and conductivity.

Sample	DF ^a	IEC ^a	WU	WU	σ	σ	σ	σ
		(meq/g)	s_c (25 °C)	H_T (25 °C)	s_c (30 °C)	H_T (30 °C) mS/cm (HCO_3^-)	s_c (60 °C) mS/cm (HCO_3^-)	H_T (60 °C) mS/cm (HCO_3^-)
QPAES-H:N [3k:2k]	2.69	2.39	85.8 ± 2.8	77.4 ± 2.3	10.1 ± 0.06	9.55 ± 0.09	22.4 ± 0.03	17.2 ± 0.06
QPAES-H:N [6k:9k]	1.09	0.97	5.50 ± 2.0	10.5 ± 2.2	2.57 ± 0.01	2.47 ± 0.05	5.61 ± 0.01	2.54 ± 0.08
QPAES-H:N [6k:5k]	2.28	2.03	58.8 ± 3.2	50.2 ± 2.7	7.34 ± 0.08	6.47 ± 0.08	15.0 ± 0.06	13.1 ± 0.06
QPAES-H:N [6k:3k]	2.88	2.56	95.7 ± 2.4	90.3 ± 1.6	16.9 ± 0.09	15.7 ± 0.04	31.4 ± 0.11	29.4 ± 0.09
QPAES-H:N [12k:31k]	0.71	0.63	3.33 ± 1.1	8.45 ± 2.4	3.01 ± 0.03	2.39 ± 0.03	6.65 ± 0.07	3.61 ± 0.07
QPAES-H:N [12k:19k]	1.43	1.27	12.0 ± 1.8	13.4 ± 1.6	1.67 ± 0.01	1.26 ± 0.03	3.98 ± 0.02	2.78 ± 0.04
QPAES-H:N [12k:11k]	2.39	2.12	78.5 ± 3.1	70.3 ± 2.9	7.97 ± 0.11	7.28 ± 0.05	15.8 ± 0.07	13.0 ± 0.06
QPAES-H:N [18k:8k]	3.17	2.82	117 ± 2.6	112 ± 3.1	15.1 ± 0.09	15.1 ± 0.07	27.9 ± 0.06	29.0 ± 0.04
QPAES-H:N [24k:39k]	0.80	0.71	11.1 ± 1.0	9.80 ± 1.1	4.67 ± 0.01	3.50 ± 0.03	6.97 ± 0.01	5.92 ± 0.08
QPAES-H:N [24k:23k]	1.76	1.56	24.5 ± 1.9	21.7 ± 2.4	3.14 ± 0.03	2.13 ± 0.03	10.2 ± 0.07	3.86 ± 0.07
QPAES-H:N [34k:14k]	3.40	3.02	177 ± 3.7	171 ± 2.5	13.8 ± 0.03	13.1 ± 0.03	24.1 ± 0.07	25.0 ± 0.07

^a Determined by ¹H NMR.

Table 3

SR of h_T and s_c QPAES-H:N [x:y] films at 25 °C and 80 °C.

Sample	SR s_c @ 25 °C	SR s_c @ 80 °C	SR h_T @ 25 °C	SR h_T @ 80 °C
QPAES-H:N [3k:2k]	21.4 ± 0.59	24.1 ± 3.21	22.9 ± 1.59	27.7 ± 2.26
QPAES-H:N [6k:9k]	4.30 ± 0.77	4.90 ± 0.18	5.00 ± 0.71	6.00 ± 0.84
QPAES-H:N [6k:3k]	24.8 ± 3.76	29.8 ± 1.14	25.7 ± 2.67	- a
QPAES-Q:N [12k:31k]	2.10 ± 0.58	3.20 ± 1.92	2.30 ± 0.73	2.60 ± 1.46
QPAES-H:N [12k:19k]	4.90 ± 0.96	5.50 ± 2.29	5.20 ± 1.53	6.40 ± 1.26
QPAES-H:N [12k:11k]	15.7 ± 2.02	18.3 ± 3.28	18.4 ± 2.74	19.0 ± 3.88
QPAES-H:N [18k:8k]	- a	- a	33.6 ± 2.79	- a
QPAES-H:N [24k:39k]	5.90 ± 2.39	6.60 ± 0.88	7.30 ± 0.48	9.30 ± 0.43
QPAES-H:N [34k:14k]	- a	- a	- a	- a

^aCould not be measured because these membranes are very brittle in the dry state.

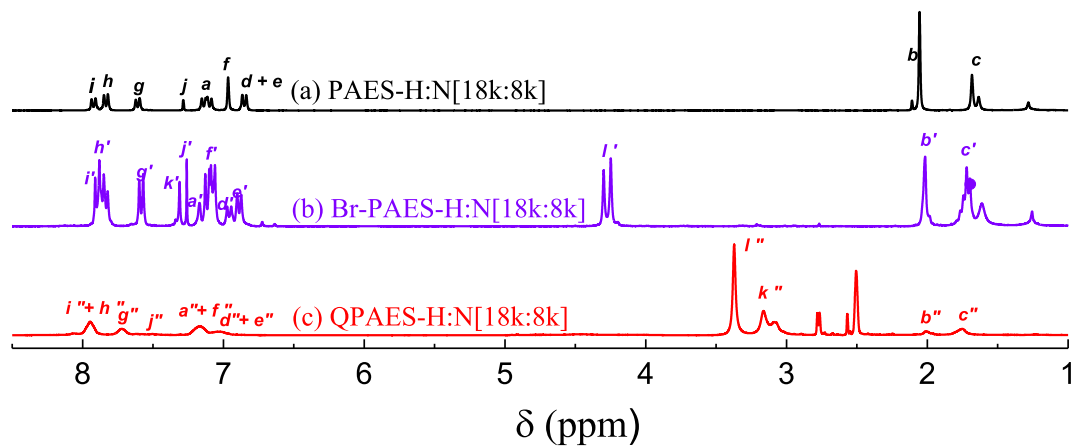


Fig. 1. ¹H NMR spectrum of (a) non-functionalized PAES-H:N [18k:8k], (b) brominated Br-PAES-H:N [18k:8k], and (c) quaternized QPAES-H:N [18k:8k].

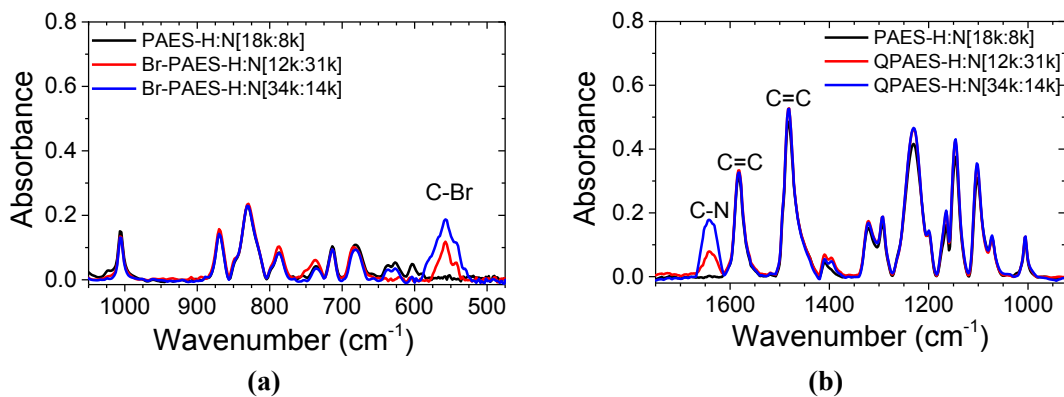


Fig. 2. FTIR spectra of (a) PAES copolymer and brominated, and (b) quaternized films.

due to its poor solubility in CDCl_3 caused by the QA group. The methyl protons (k'') of the QA group (N-CH_3) appeared at $\delta = 3.12$ ppm, and the peak at $\delta = 4.56$ ppm was assigned to the methylene protons (l'') adjacent to the QA group ($\text{Ar-CH}_2\text{-N}$). The appearance of a new peak k'' at $\delta = 3.12$ ppm and the disappearance of bromobenzyl peak at $\delta = 4.35$ ppm indicates complete material quaternization.

An example FT-IR spectra associated with functionalizing PAES-H:N [x:y] used to create a brominated and quaternized PAES-H:N [18k:8k] and PAES-H:N [12k:31k] were compared to PAES-H:N [34k:14k] shown in Fig. 2. The C-Br group associated with the bromination of PAES-H:N [x:y] occurred at 556 cm^{-1} wavenumbers. An example of this conversion is shown for low and high bromine concentration using Br-PAES-H:N [12k:31k] (IEC = 0.63) and Br-PAES-H:N [34k:14k] (IEC = 3.02) versus non-functionalized PAES-H:N [18k:8k]. An increase in C-Br intensity for Br-PAES-H:N [12k:31k] to Br-PAES-H:N [34k:14k] reveals the successful conversion of PAES-H:N [x:y] (Fig. 2a). The ionomer's C=C bonds associated with the phenyl ring at 1482 cm^{-1} were used to normalize the QPAES-H:N [12k:31k] and QPAES-H:N [34k:14k] spectra based shown in Fig. 2b. A new absorption peak at 1642 cm^{-1} is associated with the quaternary ammonium group C-N vibration for QPAES-H:N [12k:31k] and QPAES-H:N [34k:14k]. The peaks at 1580 cm^{-1} and 1482 cm^{-1} were associated with the asymmetric and symmetric phenyl ring C=C vibrations. A C-N absorption peak at 1642 cm^{-1} wavenumbers increases with quaternization. Both ^1H NMR and FT-IR results confirm the successful bromination of PAES-H:N [x:y] into Br-PAES-H:N [x:y] and quaternization using TMA to create a QPAES-H:N [x:y] film.

3.2. Ionomer film water uptake

WU is an important QA ionomer property that has profound impacts on film conductivity, dimensional stability, and mechanical strength [30,31]. A sufficient water concentration is necessary to promote the creation of ion transport channels. These channels facilitate transport through the film that produces conductivity [32]. However, excessive film WU can result in unacceptable swelling and loss of mechanical strength [33,34]. The h_T -QPAES-H:N [x:y] and s_C -QPAES-H:N [x:y] film's WU and water mass fraction ($x_{\text{H}_2\text{O}}$) are shown in Fig. 3. WU and $x_{\text{H}_2\text{O}}$ increase with IEC for heterogeneous and solution-cast films that appear to be independent of processing technique. At a lower, QA group concentration (IEC = 0.97) h_T -QPAES-H:N [6k:9k] and s_C -QPAES-H:N [6k:9k] films have a WU of 5.5 wt% ($x_{\text{H}_2\text{O}} = 0.052$) and 10.5 wt% ($x_{\text{H}_2\text{O}} = 0.062$). This is attributed to smaller water clustering within ion domains. However, as the IEC or QA group concentration increases within the

ionomer it produces larger ion domains that are able to accommodate more water. h_T -QPAES-H:N [34k:14k] and s_C -QPAES-H:N [34k:14k] film's WU was 171 wt% ($x_{\text{H}_2\text{O}} = 0.631$) and 177% ($x_{\text{H}_2\text{O}} = 0.639$) at an IEC = 3.02. Decreasing the ion block size to 18k to create QPAES-H:N [18k:8k] with a similar IEC (2.82) produced a solution-cast and heterogeneous film with a WU of 117 wt% and 112 wt%. One possible reason for QPAES-H:N [34k:14k] having a larger WU than QPAES-H:N [18k:8k] is the longer hydrophilic segment may enable a greater probability of it connecting with other ion domains. However, this speculation requires additional studies.

In general, h_T -QPAES-H:N [x:y] and s_C -QPAES-H:N [x:y] film WU characteristics appear to be quite similar and independent of pseudo-homogeneous conversion method. This could be due to the solid-state conversion process that was used to functionalize both Br-PAES-H:N [x:y] films. In order to confirm if differences exist between QA multiblock and random ionomers, an identical compositional poly (arylene ether sulfone) was created into a random QA ionomer series referred to as h_T -rQPAES. The ionomer was created using the same solid-state conversion technique as h_T -QPAES-H:N [x:y] that is shown in Fig. 3. The random ionomer had a similar IEC range as the multiblock ionomers with a slightly higher WU between an IEC of 0.5–2.0. For example, h_T -rQPAES with an IEC of 1.03 and 1.2 had a WU of 16.3 wt% and 30.7 wt% that is similar to the multiblock ionomers with an IEC = 0.97 and 1.27 with a WU of 10.5 wt% and 13.4 wt%. As previously noted, the multiblock QA ionomer film's WU continues to increase monotonically with IEC for h_T and s_C created films. However, the random QA ionomer has a WU of 223 wt% at an IEC of 2.74, whereas h_T and s_C -QPAES-H:N [18k:8k] ionomer at an IEC of 2.82 had a WU of 112 wt% and 117 wt%. These results indicate that multiblocks assemble water molecules within its structure differently than a random material, which is linked to the effective concentration of active chains (n). This was shown by Wang and Cornelius to be very important for a sulfonated pentablock ionomer with different swelling behavior due to its morphology transitioning from random to a more ordered system [12].

3.3. Ionomer film swelling

A QA ionomer film's dimensional stability and mechanical strength are closely related to swelling. In general, both solution-cast and heterogeneous QA ionomers revealed good stability. The s_C -QPAES-H:N [x:y] ionomer film's SR (change in length and width) is relatively constant after exposure to $25\text{ }^\circ\text{C}$ and $80\text{ }^\circ\text{C}$ water, which is nominally the same behavior with h_T -QPAES-H:N [x:y] films that are summarized in Table 3. For example, the SR of solution-cast and

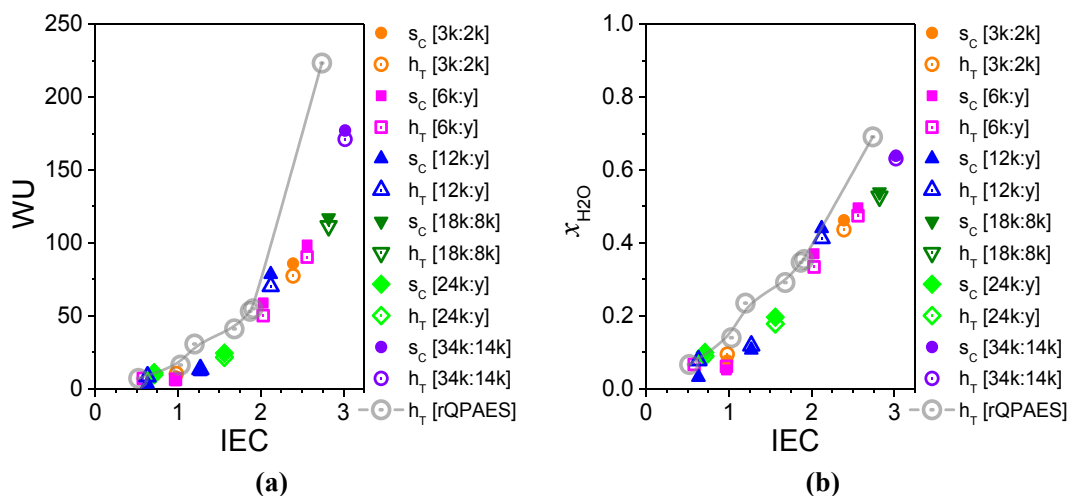


Fig. 3. QPAES-H:N [x:y] multiblock h_T and s_C , and h_T -rQPAES film's WU and x_{H_2O} versus IEC (Table 2 summarizes the standard deviation for all films).

heterogeneous QPAES-H:N [6k:3k] films was 24.8% and 25.7% at an IEC = 2.56 meq/g that is shown in Fig. 4. At low IEC, these QA ionomer films appear to have a SR that has small changes with temperature, which linearly increases with IEC. This film behavior deviates at higher functionality with an inflection near an IEC = 1.75. This type of behavior is commonly noted with sulfonated ionomers due to percolation and connection between functional groups as noted by Huang and Cornelius [13]. Overall, the smaller blocks appear to have greater SR changes than larger multiblocks. The s_C -QPAES-H:N [x:y] films had a similar SR at 25 °C and 80 °C, but its SR deviated from the linear-like trend at higher. This may be due to its larger WU due to block size and processing method.

The random rQPAES ionomers had larger SR changes with increasing IEC after soaking in water at 25 °C that became pronounced beyond an IEC of 2.0 as compared to multiblock ionomers. Its dimensional stability was immediately compromised when exposed to 80 °C water with an IEC greater than 1.75. For example, at an IEC equal to 1.91 the film's SR increased from 30.1% to 77.4%, which as a 157% change in SR with IEC that was not observed with any multiblock QA ionomer. A maximum SR for s_C and h_T QA ionomer film is 24.8% and 33.6% at 25 °C. In general, hydrophilic domains are responsible for ionomer swelling whereas hydrophobic domains impart mechanical strength and limits swelling. At low

IEC, there is a larger hydrophobic domain concentration that limits swelling due to elastic forces. As the QA hydrophilic regions increase in size and concentration that cause an equivalent change in hydrophobic domain size, which leads to greater ionomer swelling with increasing IEC. This excessive ionomer swelling prevents many interesting QA ionomer materials from being considered for applications, which involve large changes in temperature or cycling from wet to dry conditions that produce a large change in SR.

3.4. Film conductivity

The QPAES-H:N [x:y] film conductivity was measured both in the hydroxyl (OH^-) and bicarbonate form (HCO_3^-) under fully hydrated conditions at 30 °C and 60 °C. The relationship between conductivity versus IEC and water mass fraction (x_{H_2O}) for h_T and s_C films are shown in Fig. 5. The film's conductivity increases with IEC and x_{H_2O} . At low IECs (<1.18 meq/g), the h_T and s_C film conductivities were relatively low. At low IEC, QPAES-H:N [x:y] solution-cast film's conductivity is better than its heterogeneous counterpart. For example, the h_T -QPAES-H:N [24k:23k] film's hydroxyl conductivity in the HCO_3^- form is 3.14 mS/cm at IEC 1.56 meq/g, whereas its solution-cast counterpart is 10.2 mS/cm (Fig. 5a). This is approximately 3.24 times greater that may be due to better ion clustering within a solution-cast film. QA ionomers in the HCO_3^-

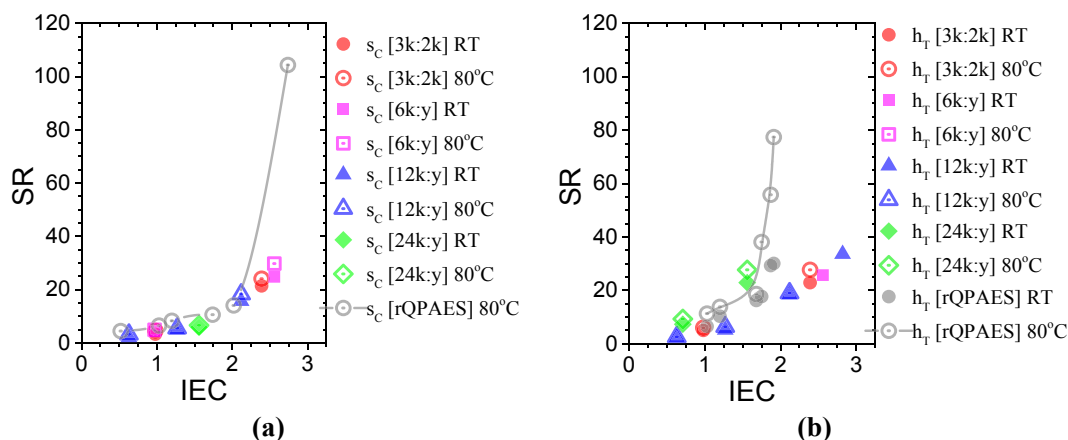


Fig. 4. SR comparison of a) s_C -QPAES-H:N [x:y], and b) h_T -QPAES-H:N [x:y] and an equivalent random PAES based QA ionomer film [35,36] (see Table 3 for standard deviation).

form with an IEC greater than 1.8 had a film conductivity that gradually increased with QA group concentration and x_{H_2O} . For example, the h_T -QPAES-H:N [34k:14k] film's conductivity at an IEC 3.02 increased from 13.1 mS/cm at 30 °C to 25.0 mS/cm at 60 °C. The s_C -QPAES-H:N [34k:14k] film had similar conductivity values of 13.8 mS/cm at 30 °C and 24.1 mS/cm at 60 °C.

Interestingly, the s_C -QPAES-Q:N [34k:14k] ionomer with the highest IEC (3.02) did not have the largest conductivity ($\sigma_{30^\circ C} = 13.8$ mS/cm and $\sigma_{60^\circ C} = 24.1$ mS/cm). Instead, the s_C -QPAES-Q:N [6k:3k] film with the smaller hydrophilic block had the largest conductivity at an IEC = 2.56 ($\sigma_{30^\circ C} = 16.9$ mS/cm and $\sigma_{60^\circ C} = 31.4$ mS/cm). The lower QPAES-Q:N [34k:14k] film conductivity is associated with a large WU (177%), and the larger hydroxyl transport occurs with the lower WU of 95.7% with QPAES-Q:N [6k:3k]. At an IEC beyond 2.5, which is equivalent to an $x_{H_2O} > 0.5$ (WU > 100%) the conductivity begins to decrease. This is believed to be a dilution effect as the concentration of QA groups per unit volume decreases due to excessive swelling, and increases the distance between functional groups. Such behavior has been reported by Park and Cornelius for AEMs et al., and by Peckham and McGrath et al. for PEMs [28,37–39]. Both Park and Peckham attributed this nonlinear trend to a dilution of the available $-N(CH_3)^+$ groups for AEMs and $-SO_3^-$ groups for PEMs caused by a significant increase in WU. A similar result was observed with Nafion based upon the number of water molecules per sulfonic acid by Gottesfeld [40]. This trend suggests that bigger hydrophilic blocks promote the creation of larger hydrophilic water domains that is noted with the WU data (Fig. 3). In general, the s_C -QPAES-H:N [x:y] film's exhibited slightly larger conductivities than h_T films. In general, the s_C -QPAES-H:N [x:y] film's exhibited slightly larger conductivities than h_T films. The larger film WU and conductivities at 60 °C are attributed to increased polymer chain mobility that produces more free volume, and improved ion diffusion.

Fig. 5b also shows a comparison of hydroxyl conductivities between random and multiblock ionomer h_T films. The multiblock ionomer conductivity ranged from 9.08 to 59.5 mS/cm and 13.7 to 119 mS/cm at 30 and 60 °C. The general hydroxyl conductivity trend for random and multiblock ionomers is that it increases with IEC. However, the random ionomers displayed lower conductivities as compared to the multiblock films both at 30 °C and 60 °C. The random h_T film with an IEC of 2.74 had conductivities of 48.7 mS/cm

and 100 mS/cm at 30 °C and 60 °C, which are 1.22 and 1.12 times lower than the multiblock h_T film with an IEC of 2.56. Moreover, the random ionomer not only exhibited lower conductivities, but also had a much higher WU (223 wt% at IEC = 2.74) as compared to its equivalent multiblock (95.7 wt% and 117 wt% at an IEC of 2.56 and 2.82). These results suggest that a random ionomer has functional groups distributed in an inefficient manner that is not as effective for ion transport.

3.5. Stress-strain analysis

QPAES-H:N [x:y] multiblock QA ionomers have soft (quaternized TBPS) and hard (BPPS) segments when they are wet, which is linked to its IEC, WU, and SR. The multiblock QA ionomer films with the least “dry” brittle behavior was the QPAES-H:N [12k:y] series. The QPAES-H:N [12k:31k], QPAES-H:N [12k:19k], and QPAES-H:N [12k:11k] wet stress-strain behavior of h_T and s_C films are shown in Fig. 6. In general, the solution-cast films exhibited significantly improved toughness and modulus compared to their heterogeneous counterparts. The Young's modulus of these QA multiblock films followed the trend of QPAES-H:N [12k:31k] > QPAES-H:N [12k:19k] > QPAES-H:N [12k:11k], and the s_C films were stiffer than

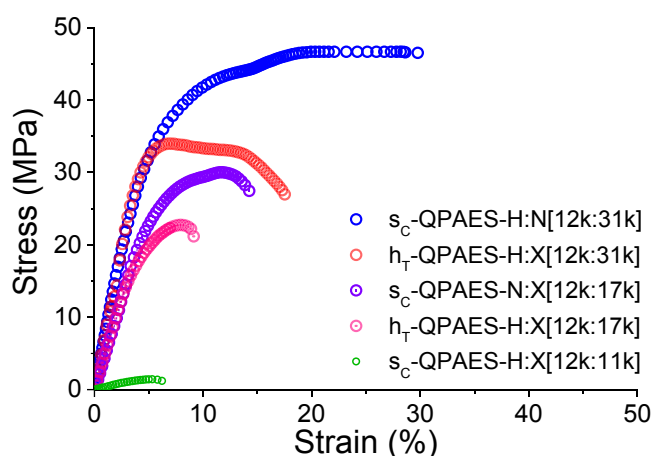


Fig. 6. Stress-strain curves of wet h_T -QPAES-H:N [x:y] and s_C -QPAES-H:N [x:y] films.

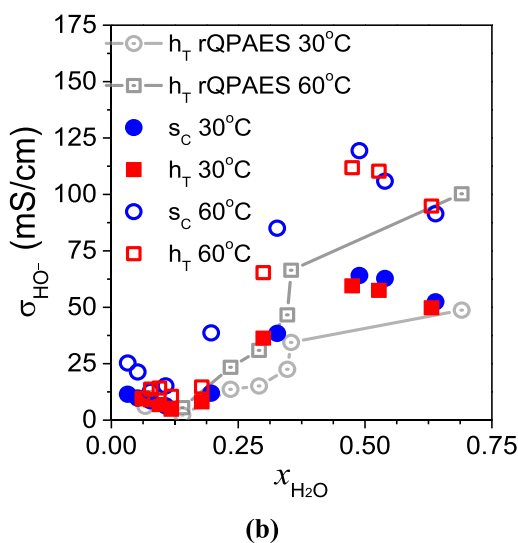
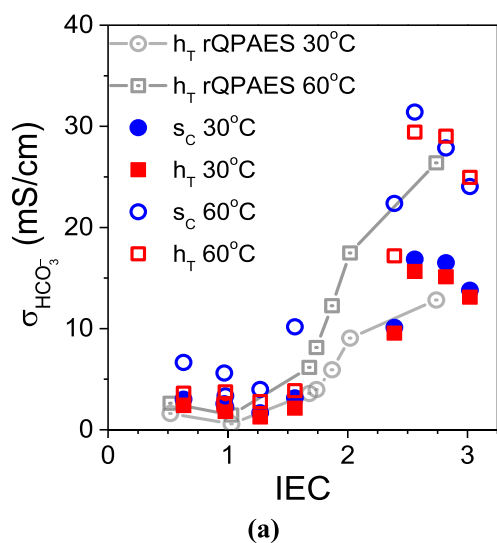


Fig. 5. QPAES-H:N [x:y] s_C and h_T film conductivity in (a) HCO_3^- form versus IEC and (b) hydroxyl conductivity versus x_{H_2O} at 30 °C and 60 °C (see Table 2 for standard deviation).

Table 4
 h_T and s_C QPAES-H:N [12k:y] film tensile properties.

Property	QPAES-H:N [12k:31k]		QPAES-H:N [12k:19k]		QPAES-H:N [12k:11k]	
	s_C	h_T	s_C	h_T	s_C	h_T
Young's Modulus (MPa)	711 ± 13.1	630 ± 11.7	492 ± 19.4	469 ± 17.2	36.0 ± 16.8	–
Elongation at break (%)	29.8 ± 4.55	15.4 ± 3.43	14.3 ± 2.41	9.14 ± 1.86	6.19 ± 1.02	–
Toughness (10 ⁴ J/m ³)	1185 ± 157	498 ± 91.7	321 ± 79.1	148 ± 67.2	5.78 ± 0.99	–

h_T ones. QPAES-H:N [12k:31k] films were 711 MPa (s_C) and 630 MPa (h_T), QPAES-H:N [12k:19k] was 492 MPa (s_C) and 469 MPa (h_T), and s_C -QPAES-H:N [12k:11k] was 36 MPa. The s_C -QPAES-H:N [12k:31k] film was tough and ductile, which is similar to a high-performance thermoplastic. This is exemplified by an ultimate elongation at break (E_b) of 29.8%, which is approximately 1.7 times larger than a h_T -QPAES-H:N [12k:31k] film (15.4%). This result is quite interesting because both films have an equivalent SR (~3%). An improved E_b film behavior was noted with s_C -QPAES-H:N [12k:19k] that had a E_b of 14.3%, which decreased to 9.14% for the heterogeneous film. A trend noted for the heterogeneous films was extreme brittleness that appeared to increase with IEC and decreased block size. Consequently, only the s_C -QPAES-H:N [12k:11k] film was measurable with an E_b of 6.19%. Overall, solution-cast films have a greater E_b than its heterogeneous counterpart.

In general, ionomer stress-strain behavior is influenced by its composition, structure, molecular weight, polydispersity (PDI), crosslinking, ionic interactions, and processing conditions (temperature, evaporation rate, solvent type, etc.). These results provide information about the Young's modulus, toughness (area under the stress-strain curve), and E_b [41]. Block copolymer stress-strain behavior is dependent upon hard and soft segment size, shape, concentration, and interconnectivity between hard and soft domains [42]. Solution-cast colloidal and heterogeneous QPAES-H:N [12k:x] films were created and mechanical properties compared to each other based upon processing technique that is summarized in Table 4. QA multiblock ionomer film's toughness varied in the following manner: QPAES-H:N [12k:31k] > QPAES-H:N [12k:19k] > QPAES-H:N [12k:11k] with s_C films being stronger than h_T ones. The improved s_C films mechanical properties may be due to a better interconnectivity between hydrophobic domains that requires additional studies. What is quite interesting about these results is the WU and SR provided no insight regarding the impact of QA ionomer film processing.

4. Conclusion

A QA poly (arylene ether sulfone) copolymer ionomer series was designed to control hydrophobic and hydrophilic block molecular weight. Block size impacted ion clustering within ionomers that altered film strength, hydroxyl transport, WU, and SR. At fully hydrated conditions, multi-block ionomers with longer hydrophilic blocks had better hydroxyl conductivity as a function of IEC as compared to its random counter-part. This was attributed to improved ion domain connectivity that was dependent upon hydrophilic block length. In general, WU increased with block length, but at a similar IEC the hydrophobic block length contributed to reducing WU and in-plane swelling if it was longer than the hydrophilic block. Ion domain interconnection was improved with increasing IEC that enhanced OH⁻ conductivity. It is speculated that local hydrophilic block reorganization in the swollen state during heterogeneous quaternization would produce a more random morphology, which exhibited lower WU and OH⁻ conductivity. This may be one reason for the large difficulty in visualizing structural

order within these materials. Multi-block QA ionomers with smaller blocks had properties similar to random copolymers at a comparable IEC. However, both conductivity and WU increased significantly with block length as observed for QPAES-H:N [12k:x] and QPAES-H:N [24k:x] multiblock copolymers. The observed WU and conductivity transition strongly suggests the formation of a more continuous hydrophilic-hydrophobic network with increasing block length. In contrast, random copolymers did not have distinct hydrophilic domains. This may be due to a greater homogeneous distribution of benzyltriethylamine groups throughout the ionomer. Based upon the copolymers investigated, the structure-property results suggest that block length should be ≥ 12 kg/mol in order to improve block spatial order and OH⁻ conductivity.

Acknowledgment

This work was possible due to funding by a grant from the Nebraska Center for Energy Sciences Research at the University of Nebraska-Lincoln enabled major portions of this work.

References

- [1] T.J. Peckham, J. Schmeisser, M. Rodgers, S. Holdcroft, Main-chain, statistically sulfonated proton exchange membranes: the relationships of acid concentration and proton mobility to water content and their effect upon proton conductivity, *J. Mater. Chem.* 17 (2007) 3255–3268.
- [2] C. Heitner-Wirguin, Recent advances in perfluorinated ionomer membranes: structure, properties and applications, *J. Membr. Sci.* 120 (1996) 1–33.
- [3] K.D. Kreuer, On the development of proton conducting polymer membranes for hydrogen and methanol fuel cells, *J. Membr. Sci.* 185 (2001) 29–39.
- [4] R.F. Silva, M. De Francesco, A. Pozio, Solution-cast Nafion[®] ionomer membranes: preparation and characterization, *Electrochim. Acta* 49 (2004) 3211–3219.
- [5] C.H. Fujimoto, M.A. Hickner, C.J. Cornelius, D.A. Loy, Ionomeric poly(phenylene) prepared by diels-alder polymerization: synthesis and physical properties of a novel polyelectrolyte, *Macromolecules* 38 (12) (2005) 5010–5016.
- [6] T. Sata, Ion Exchange Membranes: Preparation, Characterization, Modification and Application, Royal Society of Chemistry, 2007.
- [7] H. Hibbs, C.J. Cornelius, Ion transport in random and block sulfonated polyimides, *J. Mater. Sci.* 48 (3) (2013) 1303–1309.
- [8] Y. Fan, M. Zhang, R.B. Moore, C.J. Cornelius, Structure, physical properties, and molecule transport of gas, liquid, and ions within a pentablock copolymer, *J. Membr. Sci.* 464 (2014) 179–187.
- [9] W. Zheng, C.J. Cornelius, Solvent tunable multi-block ionomer morphology and its relationship to modulus, water swelling, directionally dependent ion transport, and actuator performance, *Polymer* 103 (2016) 104–111.
- [10] T.D. Largier, D. Wang, J. Mueller, C.J. Cornelius, Improving electro dialysis based water desalination using a sulfonated diels-alder poly(phenylene), *J. Membr. Sci.* 531 (2017) 103–110.
- [11] D. Wang, Y. Fang, M. Zhang, R.B. Moore, C.J. Cornelius, Ionomer solution to film solidification dependence upon solvent type and its impact upon morphology and ion transport, *Eur. Polym. J.* 97 (2017) 169–177.
- [12] D. Wang, C.J. Cornelius, Modeling ionomer swelling dynamics of a sulfonated polyphenylene, pentablock copolymers, and nafion, *J. Polym. Sci. B Polym. Phys.* 55 (5) (2017) 435–443.
- [13] F. Huang, T.D. Largier, W. Zheng, C.J. Cornelius, Pentablock ionomer solution to film morphology: impact upon ion transport, fuel cell and vanadium flow battery function, and actuator performance, *J. Membr. Sci.* 545 (2018) 1–10.
- [14] A. Eisenberg, H.L. Yeager, Perfluorinated Ionomer Membranes, Wiley, 1982.
- [15] A. Eisenberg, J.S. Kim, Introduction to Ionomers, Wiley, 1998.
- [16] R.J. Stanis, M.A. Yaklin, C.J. Cornelius, T. Takatera, A. Umemoto, A. Ambrosini, C.H. Fujimoto, Evaluation of hydrogen and methanol fuel cell performance of sulfonated diels alder polyphenylene membranes, *J. Power Sources* 195 (1)

- (2010) 104–110.
- [17] F. Huang, T.D. Largier, W. Zheng, C.J. Cornelius, Pentablock ionomer solution to film morphology: impact upon ion transport, fuel cell and vanadium flow battery function, and actuator performance, *J. Membr. Sci.* 545 (2018) 1–10.
- [18] E.E. Switzer, T.S. Olson, A.K. Datye, P. Atanassov, M.R. Hibbs, C. Fujimoto, C.J. Cornelius, Novel KOH-free anion-exchange membrane fuel cell: performance comparison of alternative anion-exchange ionomers in catalyst ink, *Electrochim. Acta* 55 (9) (2010) 3404–3408.
- [19] L.H. Sperling, *Introduction to Physical Polymer Science*, John Wiley & Sons, 2005.
- [20] V. Abetz, P.F.W. Simon, Phase behaviour and morphologies of block copolymers, *Advanced Polymer Science* 189 (2005) 125–212.
- [21] B.P. Grady, Review and critical analysis of the morphology of random ionomers across many length scales, *Polym. Eng. Sci.* 48 (2008) 1029–1051.
- [22] H.S. Lee, A.S. Badami, A. Roy, J.E. McGrath, Segmented sulfonated poly(arylene ether sulfone)-b-polyimide copolymers for proton exchange membrane fuel cells. I. Copolymer synthesis and fundamental properties, *J. Polym. Sci. Part A Polym. Chem.* 45 (2007) 4879–4890.
- [23] C. Zhao, H. Lin, K. Shao, X. Li, H. Ni, Z. Wang, H. Na, Block sulfonated poly(ether ether ketone)s (SPEEK) ionomers with high ion-exchange capacities for proton exchange membranes, *J. Power Sources* 162 (2) (2006) 1003–1009.
- [24] G.P. Robertson, D. Serguei, S.D. Mikhailenko, K. Keping Wang, P. Xing, M.D. Guiver, S. Serge Kaliaguine, Casting solvent interactions with sulfonated poly(ether ether ketone) during proton exchange membrane fabrication, *J. Membr. Sci.* 219 (2003) 113–121.
- [25] P. Bebin, H. Galiano, Processing of PEMFC membranes by extrusion: Part 1. Sulfonated polysulfone in acid form, *Adv. Polym. Technol.* 25 (2006) 121–126.
- [26] P. Bebin, H. Galiano, Processing of sulfonated polysulfone for PEMFC membrane applications: Part 2. Polymer in salt form, *Adv. Polym. Technol.* 25 (2006) 127–133.
- [27] X. Lu, W.P. Steckle, R.A. Weiss, Ionic aggregation in a block copolymer ionomer, *Macromolecules* 26 (1993) 5876–5884.
- [28] M. Lee, J.K. Park, H.S. Lee, J.E. McGrath, D.G. Baird, Effects of block length and solution-casting conditions on the final morphology and properties of disulfonated poly(arylene ether sulfone) multiblock copolymer films for proton exchange membranes, *Polymer* 50 (2009) 6129–6138.
- [29] Y. Fan, C.J. Cornelius, H.-S. Lee, J.E. McGrath, M. Zhang, R. Moore, C.L. Staiger, The effect of block length upon structure, physical properties, and transport within a series of sulfonated poly(arylene ether sulfone)s, *J. Membr. Sci.* 430 (2013) 106–112.
- [30] N. Li, Q. Zhang, C. Wang, Y.M. Lee, M.D. Guiver, Phenyltrimethylammonium functionalized polysulfone anion exchange membranes, *Macromolecules* 45 (2012) 2411–2419.
- [31] J. Wang, Z. Zhao, F. Gong, S. Li, S. Zhang, Synthesis of soluble poly(arylene ether sulfone) ionomers with pendant quaternary ammonium groups for anion exchange membranes, *Macromolecules* 42 (2009) 8711–8717.
- [32] Z. Zhang, K. Shen, L. Lin, J. Pang, Anion exchange membranes based on tetra-quaternized poly(arylene ether ketone), *J. Membr. Sci.* 497 (2016) 318–327.
- [33] K. Shen, J. Pang, S. Feng, Y. Wang, Z. Jiang, Synthesis and properties of a novel poly(aryl ether ketone)s with quaternary ammonium pendant groups for anion exchange membranes, *J. Membr. Sci.* 440 (2013) 20–28.
- [34] W. Wang, S. Wang, W. Li, X. Xie, Y. Lu, Synthesis and characterization of a fluorinated cross-linked anion exchange membrane, *Int. J. Hydrogen Energy* 38 (2013) 11045–11052.
- [35] W. Mei, C. Lu, J. Yan, Z. Wang, Anion exchange membranes by bromination of benzylmethyl-containing poly(sulfone)s, *Macromolecules* 43 (2010) 2349–2356.
- [36] X. Li, S. Cheng, L. Wang, Q. Long, J. Jinxiong Tao, G. Nie, S. Liao, Anion exchange membranes by bromination of benzylmethyl-containing poly(arylene ether)s for alkaline membrane fuel cells, *RSC Adv.* 4 (2014) 29682–29693.
- [37] T.J. Peckham, J. Schmeisser, M. Rodgers, S. Holdcroft, Main-chain, statistically sulfonated proton exchange membranes: the relationships of acid concentration and proton mobility to water content and their effect upon proton conductivity, *J. Mater. Chem.* 17 (2007) 3255–3268.
- [38] M.R. Hibbs, M.A. Hickner, T.M. Alam, S.K. McIntyre, C.H. Fujimoto, C.J. Cornelius, Transport properties of hydroxide and proton conducting membranes, *Chem. Mater.* 20 (7) (2008) 2566–2573.
- [39] D.Y. Park, P.A. Kohl, H.W. Beckham, Anion-conductive multiblock aromatic copolymer membranes: structure-property relationships, *J. Phys. Chem. C* 117 (30) (2013) 15468–15477.
- [40] S. Gottesfeld, T.A. Zawodzinski, Polymer electrolyte fuel cells, *Adv. Electrochem. Sci. Eng.* 5 (1997) 195–301.
- [41] Y. Kawano, Y. Wang, R.A. Palmer, S.R. Aubuchon, Stress-strain curves of nafion membranes in acid and salt forms, *Polímeros* 12 (2) (2002) 96–101.
- [42] J.A. Miller, S.B. Lin, K.K.S. Hwang, K.S. Wu, P.E. Gibson, S.L. Cooper, Properties of polyether-polyurethane block copolymers: effects of hard segment length distribution, *Macromolecules* 18 (1985) 32–44.